Hybrid renormalization with gradient flow for baryon quasidistribution amplitudes

Jia-Lu Zhang* and Mu-Hua Zhang

Tsung-Dao Lee Institute, Shanghai Jiao Tong University, Shanghai 201210, China and State Key Laboratory of Dark Matter Physics, School of Physics and Astronomy, Shanghai Jiao Tong University, Shanghai 200240, China

(Received 20 October 2025; accepted 11 December 2025; published 5 January 2026)

We establish a factorization relation between baryon quasidistribution amplitudes (quasi-DAs) defined with gradient flow and their counterparts renormalized in the $\overline{\mathrm{MS}}$ scheme. Working beyond the small flow-time limit, we perform a complete one-loop calculation that yields the full matching kernel and the associated Wilson-line linear divergence for flowed quasi-DAs. Building on this relation, we formulate a hybrid renormalization scheme that combines ratio scheme with gradient-flow matching, thereby replacing fit-dependent self-renormalization and improving theoretical control over scheme conversion. The framework enables a systematic connection between lattice QCD matrix elements and continuum baryon quasi-DAs, with reduced renormalization uncertainties and clear guidance for practical lattice analyses.

DOI: 10.1103/rm4s-wlfq

I. INTRODUCTION

Understanding the partonic structure of hadrons from first principles remains a central goal of quantum chromodynamics (QCD). Among the key nonperturbative quantities in this pursuit are the light-cone distribution amplitudes (LCDAs), which encode how the longitudinal momentum of a hadron is shared among its valence quarks and gluons. LCDAs play a crucial role in QCD factorization theorems for hard exclusive processes, such as meson and baryon form factors at large momentum transfer [1,2] and exclusive meson production [3]. However, because they are defined through nonlocal light-cone correlations, LCDAs are intrinsically Minkowskian and cannot be accessed directly in Euclidean lattice QCD. Their determination therefore requires indirect or alternative approaches.

A powerful strategy is to construct quasidistribution amplitudes (quasi-DAs) from equal-time correlators of boosted hadrons, which can be computed on the lattice and related to LCDAs through perturbative matching. This approach, realized in frameworks such as large momentum effective theory (LaMET) [4–6], the pseudodistribution method [7,8] and other related methods [9,10], has enabled systematically improvable studies of LCDAs [11–25] and other observables such as parton distribution functions (PDFs) and generalized parton distributions (GPDs) [6,26–28,28–67]. In recent years, this method has been successfully applied to baryon LCDAs both theoretically and numerically [11–13,17].

Despite these advances, two major challenges persist in practical lattice implementations. The first is the poor signal-to-noise ratio in nonlocal correlation functions, which becomes particularly severe at large hadron momenta and long Wilson-line separations. Reliable access to light-cone physics requires both large P and sizable z, but increasing either worsens statistical precision. The second difficulty lies in renormalization; since continuum schemes such as $\overline{\mathrm{MS}}$ cannot be implemented directly on the lattice, one must employ an intermediate nonperturbative scheme, most commonly RI/MOM [68,69]. While effective in principle, it requires a precise gauge fixing to control systematic uncertainties [70]. Alternative approaches such as self-renormalization and hybrid renormalization [71–73] mitigate some systematics but are often more complicated to implement in practice.

The gradient flow formalism [74–77] offers a promising solution to these issues. By evolving gauge and fermion fields along a fictitious fifth (flow-time) dimension governed by diffusion-like equations, the flow acts as a gauge-invariant smearing over a physical length scale $\sqrt{8t}$, where t is the flow time. It systematically suppresses ultraviolet (UV) fluctuations while preserving long-distance physics. As a result, most composite operators built from flowed

*Contact author: elpsycongr00@sjtu.edu.cn

Published by the American Physical Society under the terms of the Creative Commons Attribution 4.0 International license. Further distribution of this work must maintain attribution to the author(s) and the published article's title, journal citation, and DOI. Funded by SCOAP³.

fields are finite and well-defined at nonzero flow time, eliminating the need for additional renormalization and improving the numerical stability of correlation functions on the lattice.

Moreover, the gradient flow enhances the signal quality of nonlocal or boosted operators essential for quasidistribution studies. The smearing reduces short-distance statistical noise and improves the overlap with the ground-state signal, leading to cleaner plateaus and more precise lattice measurements. In practice, this results in improved statistical precision and better control over systematic uncertainties. Despite the smearing, flowed operators admit a well-defined perturbative expansion and can be matched to their counterparts in the $\overline{\text{MS}}$ scheme. These properties make the gradient flow a powerful tool for combining the nonperturbative strengths of lattice QCD with the analytical control of continuum perturbation theory.

The gradient-flow formalism has been extensively studied in the context of quasi-PDFs, including the establishment of factorization [78–80] and lattice implementations [81–83]. In this work, we establish the factorization relation between baryon quasi-DAs defined with gradient flow and their counterparts renormalized in the $\overline{\text{MS}}$ scheme. A complete one-loop calculation beyond the small-flow-time approximation is performed, yielding the full matching kernel and the linear divergence of the flowed quasi-DAs. Based on this relation, we propose a hybrid renormalization scheme, in which gradient-flow matching is used to convert the lattice scheme to the $\overline{\text{MS}}$ scheme, and the ratio scheme is employed to eliminate the logarithmic divergence. This framework provides a systematic and practical approach to connect lattice QCD calculations of baryon quasi-DAs with continuum observables, offering improved control over renormalization uncertainties.

The remainder of this paper is organized as follows. Section II introduces the theoretical framework, including the definitions of baryon LCDAs and quasi-DAs and the gradient flow formalism. Section III establishes the factorization relation between flowed quasi-DAs and their $\overline{\text{MS}}$ counterparts and presents the complete one-loop calculation beyond the small-flow-time approximation. Section IV develops the hybrid renormalization scheme. Section V concludes with a brief summary and outlook.

II. THEORETICAL FRAMEWORK

A. Quasi-DAs and LCDAs for baryons

The baryon LCDAs are defined through nonlocal hadron-to-vacuum matrix elements with lightlike separations [84],

$$\begin{aligned} H(z_1,z_2,z_3)_{\alpha\beta\gamma} = \epsilon^{ijk}\langle 0|f^{i'}_{\alpha}(z_1 n)W^{i'i}(z_1 n,z_0 n) \\ \times g^{j'}_{\beta}(z_2 n)W^{j'j}(z_2 n,z_0 n) \\ \times h^{k'}_{\gamma}(z_3 n)W^{k'k}(z_3 n,z_0 n)|B(P)\rangle, \end{aligned} \tag{1}$$

where $|\Lambda(P,\lambda)\rangle$ denotes the Λ baryon state with momentum P and helicity λ. The indices α, β, and γ refer to Dirac components, while f, g, and h represent the quark flavor fields. Two light-cone vectors are defined as $n^\mu = \frac{1}{\sqrt{2}}(1,0,0,-1)$ and $\bar{n}^\mu = \frac{1}{\sqrt{2}}(1,0,0,1)$, with the baryon momentum taken along the $\bar{n}$ direction, $P^\mu = P^+\bar{n}^\mu = (P^z,0,0,P^z)$. The lightlike Wilson lines W_{ij} connect the nonlocal quark fields to a common reference point z_0, ensuring gauge invariance of the operator. For simplicity, we omit the explicit Wilson lines in what follows.

The most general decomposition of Eq. (1) involves 24 invariant functions [85], but only three of them correspond to leading twist (twist 3),

$$\begin{aligned} H(z_1,z_2,z_3)_{\alpha\beta\gamma} = \frac{1}{4}f_V[(\not{P}C)_{\alpha\beta}(\gamma_5 u_\Lambda)_\gamma V(z_i P\cdot n) \\ + (\not{P}\gamma_5 C)_{\alpha\beta}(u_\Lambda)_\gamma A(z_i P\cdot n)] \\ + \frac{1}{4}f_T[(i\sigma_{\mu\nu}P^\nu C)_{\alpha\beta}(\gamma^\mu\gamma_5 u_\Lambda)_\gamma T(z_i P\cdot n)]. \end{aligned} \tag{2}$$

The individual leading-twist LCDAs can be projected by inserting appropriate Dirac matrices Γ in the nonlocal operator,

$$\begin{aligned} \Phi_{V/A/T}(z_1,z_2,\mu)P^+ f_A u_\Lambda(P) \\ = \epsilon_{ijk}\langle 0|u^{i,\mathrm{T}}(z_1 n)\Gamma d^j(z_2 n)s^k(0)|\Lambda(P)\rangle, \end{aligned} \tag{3}$$

where μ denotes the renormalization scale. In this work, we primarily focus on the axial amplitude $A(z_i P\cdot n)$, corresponding to $\Gamma = Cn/\gamma_5$. For simplicity, we set $z_3 = 0$. The momentum-space LCDA is then defined as

$$\begin{aligned} \phi_A(x_1,x_2,\mu) = \int\frac{P^+dz_1}{2\pi}\int\frac{P^+dz_2}{2\pi} \\ \times e^{i(x_1 z_1 + x_2 z_2)P^+}\Phi_A(z_1,z_2,\mu). \end{aligned} \tag{4}$$

The LCDAs can be extracted from the corresponding quasi-DAs via factorization. The quasi-DA for the A-wave is defined by

$$\begin{aligned} \tilde{\phi}_A(x_1,x_2,\mu) = \int\frac{P^z dz_1}{2\pi}\int\frac{P^z dz_2}{2\pi} \\ \times e^{-i(x_1 z_1 + x_2 z_2)P^z}\tilde{\Phi}_A(z_1,z_2,P^z,\mu), \end{aligned} \tag{5}$$

where $\tilde{\Phi}_A$ is the equal-time correlator,

$$\tilde{\Phi}_A(z_1, z_2, P^z, \mu) f_A P^\nu u_\Lambda(P) = \langle 0|u^T(z_1 n_z)(C\gamma_5\gamma^\nu) d(z_2 n_z) s(0)|\Lambda(P)\rangle, \quad (6)$$

with $n_z^\mu = (0, 0, 0, -1)$ the unit vector along the spatial z direction.

The factorization relation between the quasi-DAs and LCDAs reads

$$\tilde{\phi}_A(x_1, x_2, P^z, \mu) = \int_0^1 dy_1 \int_0^{1-y_1} dy_2 \times C(x_1, x_2, y_1, y_2, P^z, \mu)\phi_A(y_1, y_2, \mu) + \mathcal{O}\left(\frac{\Lambda_{\rm QCD}^2}{(x_1 P^z)^2}, \frac{\Lambda_{\rm QCD}^2}{(x_2 P^z)^2}, \frac{\Lambda_{\rm QCD}^2}{[(1-x_1-x_2)P^z]^2}\right), \quad (7)$$

where the power corrections are suppressed in the large-momentum limit. The perturbative matching kernel can be expanded in α_s as

$$C(x_1, x_2, y_1, y_2, P^z, \mu) = \delta(x_1 - y_1)\delta(x_2 - y_2) + \frac{\alpha_s C_F}{2\pi} c^{(1)}(x_1, x_2, y_1, y_2, P^z, \mu) + \mathcal{O}(\alpha_s^2), \quad (8)$$

where the explicit one-loop expression for $c^{(1)}$ can be found in Refs. [12,13,17].

Extracting baryon quasi-DAs on the lattice, however, remains highly challenging. Unlike the mesonic case, the baryon distribution amplitude depends on two independent momentum fractions, making it effectively a two-dimensional quantity. This feature significantly amplifies the signal-to-noise problem. In addition, the renormalization of such multivariable nonlocal operators is considerably more involved.

In our previous work, we developed a two-dimensional hybrid renormalization scheme to handle the associated mixing and divergence structure, with a detailed description provided in Refs. [12,17]. Despite its theoretical consistency, the approach remains numerically demanding. These challenges motivate the introduction of the gradient-flow formalism in the next subsection, which provides a framework to regularize and renormalize baryon quasi-DAs more efficiently.

B. Gradient flow formalism

The gradient flow provides a systematic framework for suppressing UV fluctuations in both gauge and fermion fields [74–76,86]. By evolving the fields along an auxiliary fifth dimension, the flow time t, short-distance modes are smoothed while long-range physics is preserved. Owing to these properties, the gradient flow has become an essential tool in lattice QCD, widely applied to scale setting, renormalization, and improving signal quality in hadronic observables [77,87–96].

The flow transforms the gauge field $A_\mu(x)$ and fermion field $\psi(x)$ into flowed fields $B_\mu(t, x)$ and $\chi(t, x)$, respectively, obtained by solving diffusionlike equations,

$$\begin{aligned} \partial_t B_\mu &= D_\nu G_{\nu\mu} + \kappa D_\mu \partial_\nu B_\nu, \\ \partial_t \chi &= D_\mu D_\mu \chi - \kappa(\partial_\mu B_\mu)\chi, \\ \partial_t \bar{\chi} &= \bar{\chi}\overleftarrow{D}_\mu \overleftarrow{D}_\mu + \kappa \bar{\chi}\partial_\mu B_\mu, \end{aligned} \quad (9)$$

where D_μ acts in the adjoint representation for gauge fields and in the fundamental representation for fermions. The parameter κ is a gauge-fixing term that does not affect physical observables. The flowed field-strength tensor is

$$G_{\mu\nu} = \partial_\mu B_\nu - \partial_\nu B_\mu + [B_\mu, B_\nu], \quad (10)$$

with boundary conditions

$$\begin{aligned} B_\mu(x; t = 0) &= g A_\mu(x), \\ \chi(x; t = 0) &= \psi(x), \\ \bar{\chi}(x; t = 0) &= \bar{\psi}(x). \end{aligned} \quad (11)$$

As the flow time increases, UV fluctuations are exponentially damped and the fields become smooth over a characteristic length scale $\sqrt{8t}$. Composite operators built from flowed fields, referred to as "flowed operators" are automatically UV finite at nonzero t, eliminating the need for additional counterterms. This property makes the gradient flow particularly powerful for defining renormalized operators on the lattice.

Moreover, the flow introduces a physical scale $\sqrt{8t}$ that can serve as a nonperturbative renormalization scale or as a matching scale between lattice and continuum schemes. Thus, the gradient flow simultaneously improves statistical precision and provides theoretical control over renormalization and scheme conversion.

Unlike smearing techniques such as stout smearing [86,97], which obscure perturbative structures, the gradient flow preserves the applicability of perturbation theory. The gradient flow formalism admits a well-defined expansion with modified Feynman rules [98], maintaining compatibility with continuum calculations.

In the following sections, we apply the gradient-flow formalism to baryon quasidistribution amplitudes. It serves as a replacement for self-renormalization, offering a gauge-invariant and ultraviolet-finite framework that enables a controlled conversion from the lattice scheme to the $\overline{\rm MS}$ scheme and a systematic elimination of short-distance divergences.

III. FACTORIZATION OF BARYON QUASI-DAS WITH GRADIENT FLOW

The factorization of flowed quasiobservables into their $\overline{\text{MS}}$ counterparts has been firmly established in the study of quasi-PDFs [79,80,99]. In these analyses, the gradient flow serves as a gauge-invariant framework that enables a well-defined matching of lattice observables to the $\overline{\text{MS}}$ scheme. An important outcome of these studies is that, in the small flow-time limit $t \to 0$, the matching kernel becomes free from any explicit dependence on the spatial interval.

In this section, we establish the factorization relation that connects the flowed baryon quasi-DAs to their counterparts renormalized in the $\overline{\text{MS}}$ scheme. The factorization formula reads,

$$\tilde{\Phi}^R(z_1, z_2, P^z, t) = e^{\delta m \tilde{z}} \mathcal{C}_q(t, z_1, z_2, \mu) \tilde{\Phi}^{\overline{\text{MS}}}(z_1, z_2, P^z, \mu), \tag{12}$$

where $\Phi^R(z_1, z_2, P^z, t)$ stands for the flowed quasi-DA. The factor $e^{\delta m \tilde{z}}$ represents the linear divergence arising from the self-energy corrections of the Wilson line, where [80]

$$\delta m = -\frac{\alpha_s}{4\pi} C_F \frac{\sqrt{2\pi}}{\sqrt{t}} + \mathcal{O}(\alpha_s^2), \tag{13}$$

and

$$\tilde{z} = \begin{cases} |z_1 - z_2|, & \text{if } z_1 z_2 < 0, \\ \max(|z_1|, |z_2|), & \text{if } z_1 z_2 \geq 0. \end{cases} \tag{14}$$

This matching equation isolates the short-distance effects encoded in the small flow time t into the perturbative coefficient $\mathcal{C}_q(t, z_1, z_2, \mu)$, thereby enabling a clean separation between the flow-induced ultraviolet structure and the long-distance dynamics contained in $\tilde{\Phi}^{\overline{\text{MS}}}(z_1, z_2, P^z, \mu)$.

In the $\overline{\text{MS}}$ scheme, the Wilson-line self-energy contains the UV renormalon [100,101], which manifests as a factorial growth of the perturbative coefficients at large orders. In contrast, within the gradient-flow formalism, a finite flow time t effectively removes the UV renormalon associated with this linear divergence [102].

Reference [80] suggests that, in the small flow-time limit, the matching kernel can be derived from the matching of local composite operators using the auxiliary-field method, provided that the matrix elements satisfy the condition $z \gg \sqrt{8t}$. However, for baryon LCDAs, which involve three independent spatial separations, this hierarchy is not guaranteed throughout the entire configuration space. Consequently, there exist regions where the required separation between physical scales is violated, potentially introducing uncontrolled systematic effects.

To improve the precision and reliability of the matching, we compute the full one-loop matching kernel without relying on the small flow-time approximation.

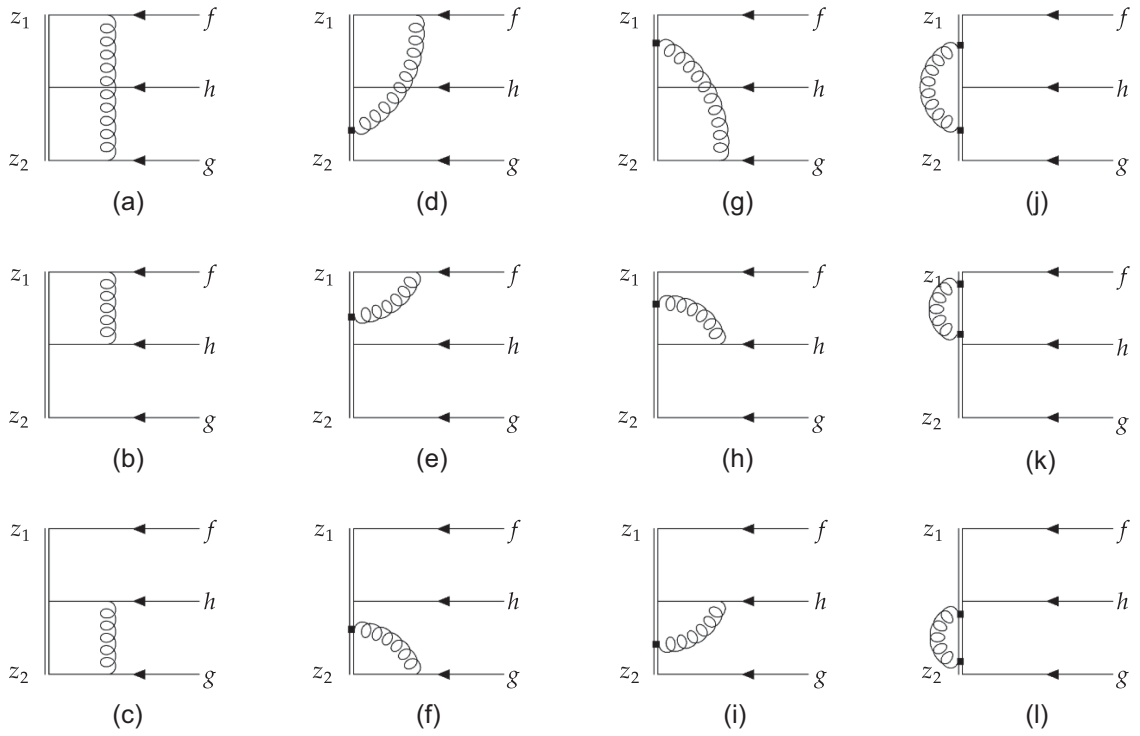


FIG. 1. (a)–(l) One-loop diagrams for the equal-time correlator $\tilde{\Phi}^R(z_1, z_2, P^z, t)$. The double line represents the Wilson line, and the filled squares mark the flowed gauge fields B_μ at flow time t.

In the following, we focus on the calculation of the A-wave of the flowed quasi-DA for the Λ baryon:

$$\tilde{\Phi}^R(z_1, z_2, P^z, t) = \langle 0|u^T(z_1, t)C\gamma^3\gamma_5 d(z_2, t)s(0, t)|\Lambda(P)\rangle. \tag{15}$$

The one-loop diagrams contributing to $\tilde{\Phi}^R(z_1, z_2, P^z, t)$ are shown in Fig. 1. Corrections to the external legs are omitted in the calculation since they cancel in the ratio scheme, which will be discussed in Sec. IV.

A. One-loop corrections for the flowed quasi-DA

Having established the factorization relation for baryon quasi-DAs with gradient flow, we now proceed to the explicit one-loop calculation of the matching kernel and the Wilson-line linear divergence. The calculation is carried out using zero-momentum external states and dimensional regularization in $d = 4 - 2\epsilon$, with renormalization performed in the $\overline{\text{MS}}$ scheme. For simplicity, we fix the gauge parameters to $\kappa = 1$ and $\xi = 1$.

To determine the matching kernel, one needs the one-loop corrections to the quasi-DA computed both in the gradient-flow scheme and in the $\overline{\text{MS}}$ scheme. The difference between these two results defines the perturbative matching coefficient $\mathcal{C}_q(t, z_1, z_2, \mu)$ in Eq. (12). Because the factorization removes only the short-distance dependence on the small flow time t, the external quark momenta, which are part of the IR dynamics, cannot appear in the perturbative matching kernel. Consequently, we evaluate $\mathcal{C}_q(t, z_1, z_2, \mu)$ with vanishing external momenta to simplify the calculation without affecting the result. Therefore, we first present the individual one-loop results in the gradient-flow and $\overline{\text{MS}}$ scheme.

We begin with the one-loop flowed gluon-exchange diagrams between external quarks, hereafter referred to as the "box diagrams," shown in Figs. 1(a)–1(c). The corresponding contributions to the flowed matrix elements are

$$\begin{aligned}
\tilde{\Phi}^R_a(z_1, z_2, P^z, t) &= \frac{C_F\alpha_s}{8\pi}\left[-\frac{1}{\epsilon_{\text{IR}}} - \log\left(\frac{1}{4}\mu^2 z_{12}^2 e^{2\gamma_E - 3}\right) + Ei(-\bar{z}_{12}^2) + \frac{3}{\bar{z}^4}(1 - e^{-\bar{z}_{12}^2}) - \frac{1}{\bar{z}^2}(4 - e^{-\bar{z}_{12}^2})\right],\\
\tilde{\Phi}^R_b(z_1, z_2, P^z, t) &= \frac{C_F\alpha_s}{16\pi}\left[-\frac{1}{\epsilon_{\text{IR}}} - \log\left(\frac{1}{4}\mu^2 z_1^2 e^{2\gamma_E - 1}\right) + Ei(-\bar{z}_1^2) - \frac{2}{\bar{z}_1^2}(1 - e^{-\bar{z}_1^2})\right],\\
\tilde{\Phi}^R_c(z_1, z_2, P^z, t) &= \frac{C_F\alpha_s}{16\pi}\left[-\frac{1}{\epsilon_{\text{IR}}} - \log\left(\frac{1}{4}\mu^2 z_2^2 e^{2\gamma_E - 1}\right) + Ei(-\bar{z}_2^2) - \frac{2}{\bar{z}_2^2}(1 - e^{-\bar{z}_2^2})\right],
\end{aligned} \tag{16}$$

while the corresponding expressions in the $\overline{\text{MS}}$ scheme are

$$\begin{aligned}
\tilde{\Phi}^{\overline{\text{MS}}}_a(z_1, z_2, P^z, \mu) &= -\frac{C_F\alpha_s}{8\pi\epsilon_{\text{IR}}} - \frac{C_F\alpha_s \log\left(\frac{1}{4}\mu^2 z_{12}^2 e^{2\gamma_E - 3}\right)}{8\pi},\\
\tilde{\Phi}^{\overline{\text{MS}}}_b(z_1, z_2, P^z, \mu) &= -\frac{C_F\alpha_s}{16\pi\epsilon_{\text{IR}}} - \frac{C_F\alpha_s \log\left(\frac{1}{4}\mu^2 z_1^2 e^{2\gamma_E - 1}\right)}{16\pi},\\
\tilde{\Phi}^{\overline{\text{MS}}}_c(z_1, z_2, P^z, \mu) &= -\frac{C_F\alpha_s}{16\pi\epsilon_{\text{IR}}} - \frac{C_F\alpha_s \log\left(\frac{1}{4}\mu^2 z_2^2 e^{2\gamma_E - 1}\right)}{16\pi}.
\end{aligned} \tag{17}$$

Here, $z_{12} \equiv z_1 - z_2$, and $\bar{z}_i \equiv z_i/\sqrt{8t}$. One can verify that, in the small flow-time limit $t \to 0$, the flowed matrix elements reduce to their corresponding expressions in the $\overline{\text{MS}}$ scheme. This behavior is consistent with expectations, as the matching kernel in this limit behaves like that of three local operators, as described in the auxiliary-field formalism [80].

Figures 1(d) and 1(g) yield no contribution to the matching kernel in the small flow-time limit for the same reason. Their flowed results are

$$\begin{aligned}
\tilde{\Phi}^R_d(z_1, z_2, P^z, t) = \frac{C_F\alpha_s}{8\pi}\Big[&\log(\bar{z}_{12}^2) - \log(\bar{z}_1^2)\\
&- Ei(-\bar{z}_{12}^2) + Ei(-\bar{z}_1^2)\\
&+ \frac{1}{\bar{z}_{12}^2}(1 - e^{-\bar{z}_{12}^2}) - \frac{1}{\bar{z}_1^2}(1 - e^{-\bar{z}_1^2})\Big],\\
\tilde{\Phi}^R_g(z_1, z_2, P^z, t) = \frac{C_F\alpha_s}{8\pi}\Big[&\log(\bar{z}_{12}^2) - \log(\bar{z}_2^2)\\
&- Ei(-\bar{z}_{12}^2) + Ei(-\bar{z}_2^2)\\
&+ \frac{1}{\bar{z}_{12}^2}(1 - e^{-\bar{z}_{12}^2}) - \frac{1}{\bar{z}_2^2}(1 - e^{-\bar{z}_2^2})\Big],
\end{aligned} \tag{18}$$

with the corresponding $\overline{\text{MS}}$ results,

$$\begin{aligned}
&\tilde{\Phi}^{\overline{\text{MS}}}_d(z_1, z_2, P^z, \mu)\\
&= \frac{C_F\alpha_s}{8\pi}\left[\log\left(z_{12}^2\mu^2 e^{2\gamma_E}\right) - \log\left(z_1^2\mu^2 e^{2\gamma_E}\right)\right],\\
&\tilde{\Phi}^{\overline{\text{MS}}}_g(z_1, z_2, P^z, \mu)\\
&= \frac{C_F\alpha_s}{8\pi}\left[\log\left(z_{12}^2\mu^2 e^{2\gamma_E}\right) - \log\left(z_2^2\mu^2 e^{2\gamma_E}\right)\right].
\end{aligned} \tag{19}$$

In the remainder of this subsection, we present the results for the remaining diagrams. Unlike the box and certain vertex diagrams, these contributions do not reduce to their corresponding expressions in the $\overline{\text{MS}}$ scheme in the small flow-time limit. Consequently, a nontrivial matching coefficient is required to relate the flowed quasi-DAs to their $\overline{\text{MS}}$ counterparts. The results for Figs. 1(e) and 1(f) are

$$\begin{aligned}\tilde{\Phi}_e^R(z_1,z_2,P^z,t) &= \frac{C_F\alpha_s}{4\pi}\left[\log\left(\bar{z}_1^2 e^{\gamma_E-1}\right)\right.\\ &\left.- Ei(-\bar{z}_1^2)+\frac{1}{\bar{z}_1^2}\left(1-e^{-\bar{z}_1^2}\right)\right],\\ \tilde{\Phi}_f^R(z_1,z_2,P^z,t) &= \frac{C_F\alpha_s}{4\pi}\left[\log\left(\bar{z}_2^2 e^{\gamma_E-1}\right)\right.\\ &\left.- Ei(-\bar{z}_2^2)+\frac{1}{\bar{z}_2^2}\left(1-e^{-\bar{z}_2^2}\right)\right],\end{aligned} \tag{20}$$

with the corresponding $\overline{\text{MS}}$ results

$$\begin{aligned}\tilde{\Phi}_e^{\overline{\text{MS}}}(z_1,z_2,P^z,\mu) &= \frac{C_F\alpha_s}{4\pi}\log\left(\frac{1}{4}\mu^2 z_1^2 e^{2\gamma_E}\right),\\ \tilde{\Phi}_f^{\overline{\text{MS}}}(z_1,z_2,P^z,\mu) &= \frac{C_F\alpha_s}{4\pi}\log\left(\frac{1}{4}\mu^2 z_2^2 e^{2\gamma_E}\right).\end{aligned} \tag{21}$$

The results for Figs. 1(h) and 1(i) are

$$\begin{aligned}\tilde{\Phi}_h^R(z_1,z_2,P^z,t) &= \frac{C_F\alpha_s}{8\pi}\left[\log\left(\bar{z}_1^2 e^{\gamma_E-1}\right)\right.\\ &\left.- Ei(-\bar{z}_1^2)+\frac{1}{\bar{z}_1^2}\left(1-e^{-\bar{z}_1^2}\right)\right],\\ \tilde{\Phi}_i^R(z_1,z_2,P^z,t) &= \frac{C_F\alpha_s}{8\pi}\left[\log\left(\bar{z}_2^2 e^{\gamma_E-1}\right)\right.\\ &\left.- Ei(-\bar{z}_2^2)+\frac{1}{\bar{z}_2^2}\left(1-e^{-\bar{z}_2^2}\right)\right],\end{aligned} \tag{22}$$

with the corresponding $\overline{\text{MS}}$ results

$$\begin{aligned}\tilde{\Phi}_h^{\overline{\text{MS}}}(z_1,z_2,P^z,\mu) &= \frac{C_F\alpha_s}{8\pi}\log\left(\frac{1}{4}\mu^2 z_1^2 e^{2\gamma_E}\right),\\ \tilde{\Phi}_i^{\overline{\text{MS}}}(z_1,z_2,P^z,\mu) &= \frac{C_F\alpha_s}{8\pi}\log\left(\frac{1}{4}\mu^2 z_2^2 e^{2\gamma_E}\right).\end{aligned} \tag{23}$$

Finally, we present the Wilson line corrections Figs. 1(j)–1(l),

$$\begin{aligned}\tilde{\Phi}_j^R(z_1,z_2,P^z,t) &= \frac{C_F\alpha_s}{4\pi}[2(e^{-\bar{z}_1^2}+e^{-\bar{z}_2^2}-e^{-\bar{z}_{12}^2})+2\sqrt{\pi}(\bar{z}_1\text{erf}(\bar{z}_1)+\bar{z}_2\text{erf}(\bar{z}_2)-\bar{z}_{12}\text{erf}(\bar{z}_{12}))\\ &\quad - Ei(-\bar{z}_{12}^2)+Ei(-\bar{z}_1^2)+Ei(-\bar{z}_2^2)-\log(\bar{z}_1^2)-\log(\bar{z}_2^2)+\log(\bar{z}_{12}^2)-\gamma_E-2],\\ \tilde{\Phi}_k^R(z_1,z_2,P^z,t) &= \frac{C_F\alpha_s}{2\pi}[-2e^{-\bar{z}_1^2}-2\sqrt{\pi}\bar{z}_1\text{erf}(\bar{z}_1)-Ei(-\bar{z}_1^2)+2\ \log(\bar{z}_1)+\gamma_E+2],\\ \tilde{\Phi}_l^R(z_1,z_2,P^z,t) &= \frac{C_F\alpha_s}{2\pi}[-2e^{-\bar{z}_2^2}-2\sqrt{\pi}\bar{z}_2\text{erf}(\bar{z}_2)-Ei(-\bar{z}_2^2)+2\ \log(\bar{z}_2)+\gamma_E+2],\end{aligned} \tag{24}$$

with the corresponding $\overline{\text{MS}}$ results

$$\begin{aligned}\tilde{\Phi}_j^{\bar{\text{MS}}}(z_1,z_2,P^z,\mu) &= \frac{C_F\alpha_s}{4\pi}\left[\log\left(\frac{1}{4}\mu^2 z_{12}^2 e^{2\gamma_E}\right)-\log\left(\frac{1}{4}\mu^2 z_1^2 e^{2\gamma_E}\right)-\log\left(\frac{1}{4}\mu^2 z_2^2 e^{2\gamma_E}\right)-2\right],\\ \tilde{\Phi}_k^{\bar{\text{MS}}}(z_1,z_2,P^z,\mu) &= \frac{C_F\alpha_s}{2\pi}\log\left(\frac{1}{4}z_1^2 e^{2\gamma_E+2}\right),\\ \tilde{\Phi}_l^{\bar{\text{MS}}}(z_1,z_2,P^z,\mu) &= \frac{C_F\alpha_s}{2\pi}\log\left(\frac{1}{4}z_2^2 e^{2\gamma_E+2}\right).\end{aligned} \tag{25}$$

The linear divergence originating from the Wilson-line self-energy becomes manifest in the gradient-flow formalism, where it is associated with the error function,

$$\text{erf}(\bar{z}) = \frac{2}{\sqrt{\pi}}\int_0^{\bar{z}} e^{-t^2}dt, \tag{26}$$

which arises from the Gaussian smearing induced by the flow. In the limit of vanishing flow time, the relation

$$\lim_{t\to 0}\bar{z}\,\text{erf}(\bar{z}) = |\bar{z}| \tag{27}$$

holds, reproducing the usual linear divergence structure. These terms correspond to the mass counterterm δm

introduced in Eq. (12). The total linear divergence from the self-energy diagrams is given by

$$\delta m\tilde{z} = -\frac{C_F\alpha_s}{2\sqrt{\pi}}(\bar{z}_1\mathrm{erf}(\bar{z}_1) + \bar{z}_2\mathrm{erf}(\bar{z}_2) + \bar{z}_{12}\mathrm{erf}(\bar{z}_{12})). \quad (28)$$

In the small flow-time limit, this expression simplifies to

$$\lim_{t\to 0}\delta m\tilde{z} = -\frac{C_F\alpha_s}{4\pi}\frac{\sqrt{2\pi}}{\sqrt{t}}\cdot\frac{|z_1| + |z_2| + |z_{12}|}{2}. \quad (29)$$

The combination $\frac{|z_1|+|z_2|+|z_{12}|}{2}$ corresponds to the effective length $\tilde{z}$ defined in Eq. (14), confirming the consistency of the flowed self-energy correction with Eq. (33).

Although most composite operators become finite under gradient flow, the flowed quark two-point function still contains a residual divergence and therefore requires renormalization. To remove this divergence, one introduces the ringed fermion field [91],

$$\mathring{\chi}(x,t) = \sqrt{\frac{-2\ \dim(R)N_f}{(4\pi)^2t^2\langle\bar{\chi}(x,t)\overleftrightarrow{\not{D}}\chi(x,t)\rangle}}\chi(x,t),$$
$$\mathring{\bar{\chi}}(x,t) = \sqrt{\frac{-2\ \dim(R)N_f}{(4\pi)^2t^2\langle\bar{\chi}(x,t)\overleftrightarrow{\not{D}}\chi(x,t)\rangle}}\bar{\chi}(x,t), \quad (30)$$

where

$$\overleftrightarrow{D}_\mu \equiv D_\mu - \overleftarrow{D}_\mu. \quad (31)$$

The ringed fermion field is finite and can be matched perturbatively to the quark field renormalized in the $\overline{\mathrm{MS}}$ scheme,

$$\mathring{\chi}(x,t) = \mathcal{C}_\chi^{1/2}(\mu,t)\psi_{\overline{\mathrm{MS}}}(x,\mu), \quad (32)$$

with the matching coefficient

$$\mathcal{C}_\chi(\mu,t) = 1 + \frac{\alpha_s}{4\pi}C_F[\ln(2\mu^2te^{\gamma_E}) - \ln(432)]. \quad (33)$$

Although the external quark self-energy cancels in our final renormalization procedure (Sec. IV), we present it here for completeness and to facilitate comparison with the auxiliary-field approach.

B. Full matching kernel

Having obtained the one-loop corrections to the flowed quasi-DA and its $\overline{\mathrm{MS}}$ counterpart, we now present the resulting matching kernel that connects the two schemes. The full matching kernel at finite flow time reads,

$$\mathcal{C}_q(z_1,z_2,t,\mu) = 1 - \frac{C_F\alpha_s}{16\pi}\Big[18\log(2\mu^2te^{\gamma_E}) + 6\log(432) + 12 + 7Ei(-\bar{z}_1^2) + 7Ei(-\bar{z}_2^2) + 6Ei(-\bar{z}_{12}^2)$$
$$+ 8(e^{-\bar{z}_1^2} + e^{-\bar{z}_2^2} + e^{-\bar{z}_{12}^2}) + \frac{2(e^{-\bar{z}_1^2}-1)}{\bar{z}_1^2} + \frac{2(e^{-\bar{z}_2^2}-1)}{\bar{z}_2^2} + \frac{6(e^{-\bar{z}_{12}^2}-1)}{\bar{z}_{12}^4} + \frac{2(e^{-\bar{z}_{12}^2}+2)}{\bar{z}_{12}^2}\Big] + \mathcal{O}(\alpha_s^2), \quad (34)$$

and in the small flow-time limit it reduces to

$$\lim_{t\to 0}\mathcal{C}_q(z_1,z_2,t,\mu) = 1 - \frac{3C_F\alpha_s}{8\pi}[3\log(2\mu^2te^{\gamma_E}) + 2 + \log(432)] + \mathcal{O}(\alpha_s^2). \quad (35)$$

It has been shown in Ref. [80] that, by introducing auxiliary fields, the matching of a nonlocal operator in the small flow-time limit can be reduced to that of local operators. In particular, the equal-time operator in Eq. (6) can be rewritten as

$$\bar{h}_v u_\alpha(z_1n_z)(C\not{n}\gamma_5)_{\alpha\beta}\bar{h}_v d_\beta(z_2n_z)\bar{h}_v s_\gamma(z_3n_z), \quad (36)$$

where $h_v(x)$ is the auxiliary quark field that effectively replaces the Wilson line. The matching kernel then depends only on the local bilinear combinations $\bar{h}_v\psi(z_in_z)$ and is independent of the spinor structure or spatial separations. The coefficient for a single $\bar{h}_v\psi(z_in_z)$ takes the form

$$\lim_{t\to 0}\mathcal{C}_{\bar{h}_v\psi}(z_1,z_2,t,\mu) = 1 - \frac{C_F\alpha_s}{8\pi}[3\log(2\mu^2te^{\gamma_E}) + 2 + \log(432)] + \mathcal{O}(\alpha_s^2), \quad (37)$$

which is exactly one-third of Eq. (35).

However, for baryon LCDAs, which depend on two independent spatial separations, the hierarchy $|z_1|, |z_2|, |z_1 - z_2| \gg \sqrt{8t}$ is not always satisfied. Consequently, deviations arise in regions where this separation of scales breaks down. Figure 2 compares the full matching kernel with its small-flow-time limit. In Fig. 2(a), we fix $\bar{z}_1 = 1$ and $\bar{z}_2 = 2$ and vary t from 0 to 0.2 fm^2; in Fig. 2(b), we show the ratio $\mathcal{C}_q(z_1,z_2,\mu,t)/\lim_{t\to 0}\mathcal{C}_q(z_1,z_2,\mu,t)$ as a function of $\bar{z}_1$ for $t = 0.03$ fm^2. The renormalization scale μ is chosen such that $\log(2e^{2\gamma_E}\mu^2t) = 0$.

One can observe two peaks where the ratio significantly deviates from unity, corresponding to the cases $z_1 = z_2$ and $z_2 = 0$. However, these deviations can be removed in the

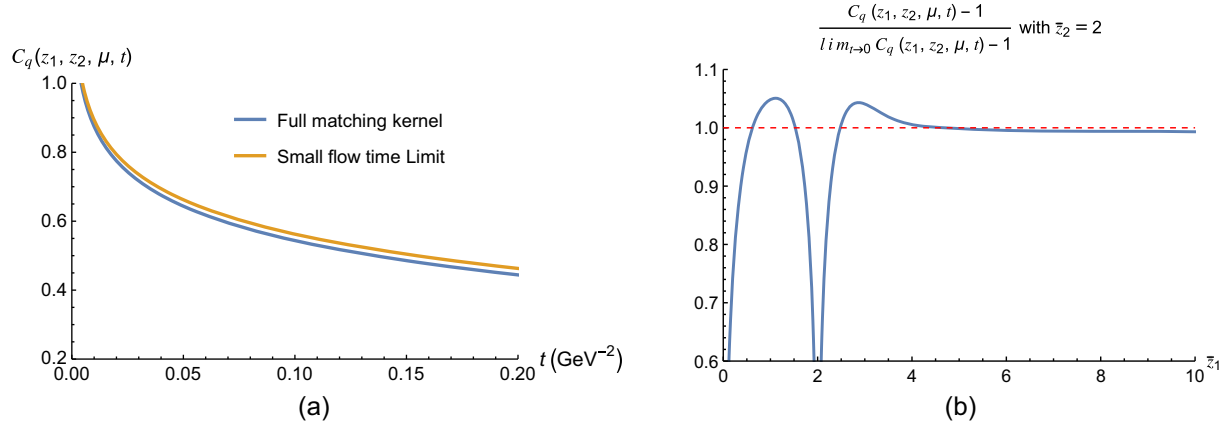


FIG. 2. (a) Variation of the matching kernel with the flow time t for fixed parameters $\bar{z}_1 = 1$, $\bar{z}_2 = 2$, and $\mu = 2$ GeV. The blue curve shows the full matching kernel, while the red curve indicates its small flow-time limit. (b) $\frac{C_q(z_1,z_2,\mu,t)-1}{\lim_{t\to 0} C_q(z_1,z_2,\mu,t)-1}$, showing the ratio of the one-loop correction of the full matching kernel to its small flow-time limit, with $\bar{z}_2 = 2$ and $t = 0.03$ fm^2. The renormalization scale μ is chosen such that $\log(2e^{2\gamma_E}\mu^2 t) = 0$.

ratio scheme, provided that the dependence on the coordinates z_i factorizes to all orders. In particular, if such factorization holds, the flowed quasi-DAs in coordinate space, in the limit of small spatial separation, can be written in the form $f_1(z_1)f_2(z_2)f_3(z_1 - z_2)$. The ratio scheme then cancels the functions $f_i(z_i)$ for small z_i by forming ratios with matrix elements that share the same functional dependence, effectively eliminating these contributions.

IV. HYBRID RENORMALIZATION

In Sec. II, we introduced the factorization relation connecting quasi-DAs and LCDAs. We note that the matching in Eq. (7) for quasi-DAs in the $\overline{\mathrm{MS}}$ scheme presents a subtle problem. This issue arises from the structure of the double plus function in the matching kernel, which contains integrals over the momentum fractions x_1' and x_2' originating from the virtual corrections to DAs [13]. In the limits $x_1', x_2' \to \infty$, these integrals behave asymptotically as $\int dx'/x'$, leading to logarithmic UV divergences. Although the complete matching kernel should include both real and virtual contributions to cancel these divergences, previous derivations often relied solely on the real diagrams, assuming that the virtual terms could be reconstructed through integration. As a result, a residual UV divergence remains, rendering a problematic definition of the double plus function.

In Ref. [6], a properly defined plus function for quasi-PDFs was introduced by performing subtractions at infinite momentum. For quasi-DAs, Ref. [13] proposed using the RI/MOM renormalization scheme to subtract these asymptotic contributions, making the plus function well defined. However, as shown in Ref. [70], it requires precise gauge fixing to properly control systematic uncertainties.

To eliminate large logarithms and convert lattice regularization to a continuum scheme, the hybrid renormalization scheme was introduced. It combines the ratio scheme and the self-renormalization scheme. The ratio scheme removes large logarithmic terms such as $\ln z_1^2$, $\ln z_2^2$, and $\ln(z_1 - z_2)^2$ that appear as $z_i \to 0$ [7,103,104]. In this approach, bare matrix elements are divided by corresponding zero-momentum matrix elements according to the spatial region (z_1, z_2). The division of regions is illustrated in Fig. 3, and a detailed application of this scheme to the baryon case can be found in Ref. [17].

The self-renormalization factor, on the other hand, converts lattice-regularized matrix elements to the $\overline{\mathrm{MS}}$ scheme [71]. It is given by

$$\begin{aligned} Z_R(z_1, z_2, a, \mu) = \exp\Bigg[&\left(\frac{k}{a\ln[a\Lambda_{\mathrm{QCD}}]} - m_0\right)\tilde{z} \\ &+ \frac{\gamma_0}{b_0}\ln\left(\frac{\ln[1/(a\Lambda_{\mathrm{QCD}})]}{\ln[\mu/\Lambda_{\overline{\mathrm{MS}}}]}\right) \\ &+ \ln\left(1 + \frac{d}{\ln(a\Lambda_{\mathrm{QCD}})}\right) + f(z_1, z_2)a\Bigg], \end{aligned} \tag{38}$$

where the parameters k, m_0, Λ_{QCD}, $f(z_1, z_2)$, and d are determined from zero-momentum matrix elements.

Using this renormalization factor, the lattice matrix element can be converted to the $\overline{\mathrm{MS}}$ scheme over the full kinematic range as

$$\tilde{\Phi}^{\overline{\mathrm{MS}}}(z_1, z_2, P^z, \mu) = \frac{\tilde{\Phi}(z_1, z_2, P^z, a)}{Z_R(z_1, z_2, a, \mu)}. \tag{39}$$

Although Z_R is extracted from zero-momentum matrix elements, it can be applied to large-momentum matrix

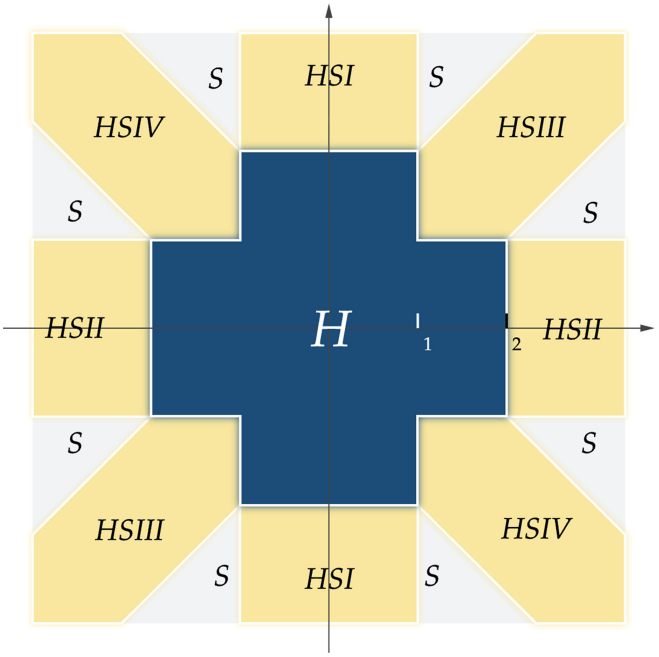


FIG. 3. Schematic diagram of the renormalization procedure. First, both large-momentum and zero-momentum matrix elements are converted to the $\overline{\mathrm{MS}}$ scheme using the gradient-flow formalism. Then, ratios are formed using these $\overline{\mathrm{MS}}$-renormalized matrix elements; the large-momentum matrix element in the blue (hard) region is divided by the zero-momentum element in the same region, the large-momentum matrix element in the yellow (hard-soft) region is divided by the zero-momentum element on the blue-yellow boundary, and the large-momentum matrix element in the gray (soft) region is divided by the zero-momentum element at the gray-yellow intersection.

elements since the renormalization factor is independent of the external states.

Although the conventional hybrid scheme has been successfully applied in previous lattice studies, it still suffers from several limitations in practice. First, due to the two-dimensional nature of baryon quasi-DAs, the extraction of matrix elements from lattice simulations suffers from a poor signal-to-noise ratio, especially at large separations in the two-dimensional coordinate space. Second, the self-renormalization procedure requires fitting the parameters in Eq. (38), which introduces additional systematic uncertainties and dependence on the chosen fitting range.

To overcome these issues, we propose an improved hybrid renormalization scheme in which gradient flow matching replaces self renormalization. This substitution improves the signal-to-noise ratio of nonlocal correlators and enables a direct, theoretically controlled matching to the $\overline{\mathrm{MS}}$ scheme. In the next subsection, we formalize the gradient-flow based hybrid renormalization and detail its implementation in lattice simulations.

A. Hybrid renormalization with gradient flow

Building on the one loop factorization with gradient flow, we now specify the hybrid renormalization used in our analysis. In this scheme, the scheme conversion is performed directly with the flowed matching relation, avoiding the fit-dependent self-renormalization. Using Eq. (12) together with Eq. (34), we replace the self-renormalization factor by

$$\tilde{\Phi}^{\overline{\mathrm{MS}}}(z_1, z_2, P^z, \mu) = e^{-\delta m \tilde{z}} \frac{\tilde{\Phi}^R(z_1, z_2, P^z, a)}{\mathcal{C}_q(t, z_1, z_2, \mu)}. \quad (40)$$

For convenience, we define the normalized matrix element

$$\hat{\Phi}^{\overline{\mathrm{MS}}}(z_1, z_2, P^z, a) = \frac{\tilde{\Phi}^{\overline{\mathrm{MS}}}(z_1, z_2, P^z, a)}{\tilde{\Phi}^{\overline{\mathrm{MS}}}(0, 0, P^z, a)}. \quad (41)$$

We now specify the hybrid renormalization used in our analysis, which combines gradient flow matching with ratio renormalization. A schematic partition of the (z_1, z_2) plane is shown in Fig. 3. For notational convenience we treat the four absolute separations $|z_1|, |z_2|, |z_1 - z_2|$, and $|z_1 + z_2|$ as "arguments" that determine the region; the last of these, $|z_1 + z_2|$, is an auxiliary scale introduced only to ensure continuity of the construction near the $z_1 \sim -z_2$ diagonal (it is not a physical scale of the baryon LCDA).

We adopt a single hybrid cutoff z_s satisfying $a \ll 2z_s \ll \Lambda_{\mathrm{QCD}}^{-1}$.

(i) *Blue (perturbative):* all relevant arguments satisfy $|z| < z_s$;
(ii) *Yellow (mixed):* one argument satisfies $|z| < z_s$;
(iii) *Gray (nonperturbative):* all arguments satisfy $|z| \geq z_s$.

The prescription proceeds case by case, always applied to the normalized matrix element $\hat{\Phi}^{\overline{\mathrm{MS}}}$ in Eq. (41). Step functions select the appropriate region and the denominator is chosen so that short-distance logarithms cancel while avoiding additional nonperturbative contamination.

(i) *All perturbative.* If z_1, z_2, and $z_1 - z_2$ are all perturbative, e.g. $(|z_1| < z_s, |z_2| < z_s)$, or $(|z_1| < z_s, z_s < |z_2| < 2z_s)$, or $(z_s < |z_1| < 2z_s, |z_2| < z_s)$—the purple/blue region in Fig. 3—we apply

$$\hat{\Phi}^{\mathrm{H}}(z_1, z_2, P^z, \mu) = \frac{\hat{\Phi}^{\overline{\mathrm{MS}}}(z_1, z_2, P^z, \mu)}{\hat{\Phi}^{\overline{\mathrm{MS}}}(z_1, z_2, 0, \mu)} (\theta(2z_s - |z_1|)\theta(z_s - |z_2|) + \theta(z_s - |z_1|)\theta(|z_2| - z_s)\theta(2z_s - |z_2|)), \quad (42)$$

with z_s as above. This ratio removes logarithms $\ln z_1^2$, $\ln z_2^2$, and $\ln(z_1-z_2)^2$, preserves normalization, and reduces discretization effects ($a \ll z_s$), yielding a conserved matching kernel after Fourier transformation;

(ii) z_1 *perturbative.* If z_1 is perturbative while z_2 and z_1-z_2 are not (e.g., $|z_1|<z_s$, $|z_2|>2z_s$)—the blue vertical band in Fig. 3—we use

$$\hat{\Phi}^{\mathrm{H}}(z_1,z_2,P^z,\mu)=\frac{\hat{\Phi}^{\overline{\mathrm{MS}}}(z_1,z_2,P^z,\mu)}{\hat{\Phi}^{\overline{\mathrm{MS}}}(z_1,\mathrm{sign}(z_2)2z_s,0,\mu)}\times\theta(z_s-|z_1|)\theta(|z_2|-2z_s), \quad (43)$$

so that $\ln z_1^2$ cancels without injecting extra long-distance structure;

(iii) z_2 *perturbative.* If z_2 is perturbative while z_1 and z_1-z_2 are not (e.g. $|z_1|>2z_s$, $|z_2|<z_s$)—the blue horizontal band—we use

$$\hat{\Phi}^{\mathrm{H}}(z_1,z_2,P^z,\mu)=\frac{\hat{\Phi}^{\overline{\mathrm{MS}}}(z_1,z_2,P^z,\mu)}{\hat{\Phi}^{\overline{\mathrm{MS}}}(\mathrm{sign}(z_1)2z_s,z_2,0,\mu)}\times\theta(|z_1|-2z_s)\theta(z_s-|z_2|); \quad (44)$$

(iv) z_1-z_2 *perturbative.* If both z_1 and z_2 are nonperturbative while z_1-z_2 is perturbative (e.g. $|z_1|>z_s$, $|z_2|>z_s$, $|z_1-z_2|<z_s$)—the blue diagonal near $z_1\sim z_2$—we take

$$\hat{\Phi}^{\mathrm{H}}(z_1,z_2,P^z,\mu)=\frac{\hat{\Phi}^{\overline{\mathrm{MS}}}(z_1,z_2,P^z,\mu)}{\hat{\Phi}^{\overline{\mathrm{MS}}}(z_1^*,z_2^*,0,\mu)}\times\theta(|z_1|-z_s)\theta(|z_2|-z_s)\times\theta(z_s-|z_1-z_2|), \quad (45)$$

with $z_1^*=z_s+(z_1-z_2)\theta(z_1-z_2)$ and $z_2^*=z_s+(z_2-z_1)\theta(z_2-z_1)$. This cancels $\ln(z_1-z_2)^2$;

(v) z_1+z_2 *(auxiliary) perturbative.* For $|z_1|>z_s$, $|z_2|>z_s$, and $|z_1+z_2|<z_s$—the blue diagonal around $z_1\sim -z_2$—we define

$$\hat{\Phi}^{\mathrm{H}}(z_1,z_2,P^z,\mu)=\frac{\hat{\Phi}^{\overline{\mathrm{MS}}}(z_1,z_2,P^z,\mu)}{\hat{\Phi}^{\overline{\mathrm{MS}}}(z_1^{**},z_2^{**},0,\mu)}\times\theta(|z_1|-z_s)\theta(|z_2|-z_s)\times\theta(z_s-|z_1+z_2|), \quad (46)$$

with $z_1^{**}=z_s+(z_1+z_2)\theta(z_1+z_2)$ and $z_2^{**}=-z_s+(z_2+z_1)\theta(-z_2-z_1)$. We emphasize that $|z_1+z_2|$ is introduced only to maintain continuity of the ratio construction; it has no direct physical interpretation in the LCDA;

(vi) *All nonperturbative.* Finally, if $|z_1|>z_s$, $|z_2|>z_s$, $|z_1-z_2|>z_s$, and $|z_1+z_2|>z_s$ (gray region), we revert to a fixed short-distance normalization point and write

$$\hat{\Phi}^{\mathrm{H}}(z_1,z_2,P^z,\mu)=\frac{\hat{\Phi}^{\overline{\mathrm{MS}}}(z_1,z_2,P^z,\mu)}{\hat{\Phi}^{\overline{\mathrm{MS}}}(\mathrm{sign}(z_1)z_s,\mathrm{sign}(z_2)2z_s,0,\mu)}\times\theta(|z_1|-z_s)\theta(|z_2|-z_s)\times\theta(|z_1-z_2|-z_s)\theta(|z_1+z_2|-z_s). \quad (47)$$

The continuity of the hybrid-renormalized quasi-DA can be checked by observing that, when crossing the boundaries between different regions, the numerator of the ratio varies smoothly and remains continuous. A detailed discussion of the hybrid renormalization scheme can be found in Refs. [12,17,105]. With the hybrid-renormalized matrix element $\hat{\Phi}^{\mathrm{H}}(z_1,z_2,P^z,\mu)$ defined above, the matching to baryon LCDAs is performed using Eq. (7). The corresponding hybrid matching kernel is given in Refs. [12,17].

We emphasize that, in the small flow-time limit, the flowed matching kernel $\mathcal{C}_q(t,z_1,z_2,\mu)$ becomes independent of the spatial separations [cf. Eq. (35)]. Consequently, $\mathcal{C}_q$ drops out in the definition of the hybrid-renormalized matrix elements when the small flow-time form is used. However, a major complication of the baryon quasi-DA is that it is a genuinely two-dimensional distribution. As a result, there are regions (the yellow regions) where perturbative and nonperturbative physics are inevitably mixed. In order to eliminate the large logarithms $\ln(\mu^2 z_i^2)$, the denominator in the hybrid ratio has to be chosen such that it carries the same large logarithms as the numerator, while the perturbative calculation remains reliable. This is precisely where the auxiliary scale z_s enters; it must satisfy $\sqrt{8t}\ll z_s\ll\frac{1}{\Lambda_{\mathrm{QCD}}}$. On the lattice this condition leaves only a rather narrow window for the admissible flow time. For lattice implementations it is therefore more reliable to employ the full matching kernel at finite flow time, which relaxes the constraint $\sqrt{8t}\ll z_s$.

B. Lattice implementation of gradient flow

In lattice simulations one works at fixed physical flow time $t>0$ with smearing radius $r_{\mathrm{sm}}=\sqrt{8t}$, and the continuum limit is taken at fixed t. For baryon quasi-DAs, all separations should simultaneously satisfy

$$\frac{1}{a}\gg\frac{1}{\sqrt{8t}}\gg\frac{1}{|z_s|},\frac{1}{|z_1|},\frac{1}{|z_2|},\frac{1}{|z_1-z_2|}, \quad (48)$$

so that flow-induced artifacts and discretization effects are parametrically separated from the operator scales. After the

continuum extrapolation at fixed t, conversion to the $\overline{\text{MS}}$ scheme can be performed using Eq. (12) with the one-loop kernel in Eq. (34), evaluated at the same t. To minimize logarithms in the matching coefficients, one may choose the renormalization scale such that $\log(2e^{2\gamma_E}\mu^2 t) = 0$.

The Wilson-line linear divergence is encoded in the factor $e^{\delta m z}$, with δm given by Eq. (33). Although this expression is derived analytically at one loop, higher-order and nonperturbative effects can modify the effective slope. Accordingly, in practice one fits the linear divergence across several flow times t, using the one-loop form as a physics-motivated prior. Finally, within a window where $t\Lambda^2_{\text{QCD}} \ll 1$ and $|z_1|, |z_2|, |z_1 - z_2| \gg r_{\text{sm}}$, a controlled extrapolation $t \to 0$ can be performed. One should note that the matching kernel is plagued by a linear renormalon [102], which can be treated using leading renormalon resummation [34].

V. SUMMARY AND OUTLOOK

We presented a systematic gradient-flow based framework to extract baryon LCDAs from lattice QCD. We established a factorization relation connecting flowed quasi-DAs to their $\overline{\text{MS}}$ counterparts and carried out a complete one-loop calculation beyond the small flow-time limit, obtaining the full matching kernel together with the Wilson-line linear divergence. Building on these results, we defined a hybrid renormalization scheme that combines ratio renormalization with gradient-flow matching, providing a numerically stable and theoretically controlled alternative to self-renormalization for lattice applications. Our future work will focus on obtaining lattice results using this approach.

ACKNOWLEDGMENTS

We thank Prof. Wei Wang and Prof. Nora Brambilla for valuable discussions. This work is supported in part by the National Natural Science Foundation of China under Grant No. 12305103. Jia-Lu Zhang is supported by the T. D. Lee scholarship.

DATA AVAILABILITY

No data were created or analyzed in this study.

[1] G. P. Lepage and S. J. Brodsky, Phys. Rev. D **22**, 2157 (1980).
[2] V. L. Chernyak and A. R. Zhitnitsky, Phys. Rep. **112**, 173 (1984).
[3] L. Mankiewicz, G. Piller, and T. Weigl, Eur. Phys. J. C **5**, 119 (1998).
[4] X. Ji, Phys. Rev. Lett. **110**, 262002 (2013).
[5] X. Ji, Sci. China Phys. Mech. Astron. **57**, 1407 (2014).
[6] T. Izubuchi, X. Ji, L. Jin, I. W. Stewart, and Y. Zhao, Phys. Rev. D **98**, 056004 (2018).
[7] A. V. Radyushkin, Phys. Rev. D **96**, 034025 (2017).
[8] A. V. Radyushkin, Phys. Rev. D **100**, 116011 (2019).
[9] Y. Q. Ma and J. W. Qiu, Phys. Rev. D **98**, 074021 (2018).
[10] Y. Q. Ma and J. W. Qiu, Phys. Rev. Lett. **120**, 022003 (2018).
[11] C. Han and J. Zhang, Phys. Rev. D **109**, 014034 (2024).
[12] C. Han, W. Wang, J. Zeng, and J. L. Zhang, J. High Energy Phys. 07 (2024) 019.
[13] Z. F. Deng, C. Han, W. Wang, J. Zeng, and J. L. Zhang, J. High Energy Phys. 07 (2023) 191.
[14] C. Han, W. Wang, J. L. Zhang, and J. H. Zhang, Phys. Rev. D **110**, 094038 (2024).
[15] W. Wang, X. Y. Han, J. Hua, X. Ji, C. D. Lü, A. Schäfer, Y. Su, J. Xu, Y. Yang, and J. H. Zhang *et al.*, Proc. Sci. QCHSC24 (**2025**) 111 [arXiv:2504.02453].
[16] M. H. Chu *et al.* (Lattice Parton Collaboration), Phys. Rev. D **111**, 034510 (2025).
[17] C. Han, Y. Su, W. Wang, and J. L. Zhang, J. High Energy Phys. 12 (2023) 044.
[18] S. M. Hu, W. Wang, J. Xu, and S. Zhao, Phys. Rev. D **109**, 034001 (2024).
[19] J. Hua *et al.* (Lattice Parton Collaboration), Phys. Rev. Lett. **129**, 132001 (2022).
[20] J. Hua, M.-H. Chu, P. Sun, W. Wang, J. Xu, Y.-B. Yang, J.-H. Zhang, and Q.-A. Zhang (Lattice Parton Collaboration), Phys. Rev. Lett. **127**, 062002 (2021).
[21] W. Wang, Y. M. Wang, J. Xu, and S. Zhao, Phys. Rev. D **102**, 011502 (2020).
[22] W. Wang, J. Xu, Q. A. Zhang, and S. Zhao, arXiv:2411.07101.
[23] X. Y. Han *et al.* (Lattice Parton Collaboration), Phys. Rev. D **111**, 034503 (2025).
[24] X. Y. Han, J. Hua, X. Ji, C. D. Lü, W. Wang, J. Xu, Q. A. Zhang, and S. Zhao, Phys. Rev. D **111**, L111503 (2025).
[25] V. M. Braun, A. Vladimirov, and J. H. Zhang, Phys. Rev. D **99**, 014013 (2019).
[26] M. H. Chu *et al.* ***(Lattice Parton (LPC) Collaboration), Phys. Rev. D **106**, 034509 (2022).
[27] T. Guo, C. Han, W. Wang, and J. L. Zhang, Phys. Rev. D **112**, 016013 (2025).
[28] W. Wang, J. Xu, Q. A. Zhang, and S. Zhao, Phys. Rev. D **112**, 054044 (2025).
[29] M. H. Chu *et al.* (Lattice Parton Collaboration), Phys. Rev. D **109**, L091503 (2024).
[30] J. C. He, M.-H. Chu, J. Hua, X. Ji, A. Schäfer, Y. Su, W. Wang, Y.-B. Yang, J.-H. Zhang, and Q.-A. Zhang (Lattice Parton Collaboration (LPC)), Phys. Rev. D **109**, 114513 (2024).

[31] Z. F. Deng, W. Wang, and J. Zeng, J. High Energy Phys. 09 (2022) 046.
[32] Q. A. Zhang, J. Hua, Y. Huo, X. Ji, Y. Liu, Y.-S. Liu, M. Schlemmer, A. Schäfer, P. Sun, W. Wang, and Y.-B. Yang (Lattice Parton Collaboration), Phys. Rev. Lett. **125**, 192001 (2020).
[33] W. Wang, J. H. Zhang, S. Zhao, and R. Zhu, Phys. Rev. D **100**, 074509 (2019).
[34] R. Zhang, J. Holligan, X. Ji, and Y. Su, Phys. Lett. B **844**, 138081 (2023).
[35] X. Xiong, X. Ji, J. H. Zhang, and Y. Zhao, Phys. Rev. D **90**, 014051 (2014).
[36] H. W. Lin, J. W. Chen, S. D. Cohen, and X. Ji, Phys. Rev. D **91**, 054510 (2015).
[37] C. Alexandrou, K. Cichy, V. Drach, E. Garcia-Ramos, K. Hadjiyiannakou, K. Jansen, F. Steffens, and C. Wiese, Phys. Rev. D **92**, 014502 (2015).
[38] J. W. Chen, S. D. Cohen, X. Ji, H. W. Lin, and J. H. Zhang, Nucl. Phys. **B911**, 246 (2016).
[39] C. Alexandrou, K. Cichy, M. Constantinou, K. Hadjiyiannakou, K. Jansen, F. Steffens, and C. Wiese, Phys. Rev. D **96**, 014513 (2017).
[40] C. Alexandrou, K. Cichy, M. Constantinou, K. Jansen, A. Scapellato, and F. Steffens, Phys. Rev. Lett. **121**, 112001 (2018).
[41] J. W. Chen, L. Jin, H. W. Lin, Y. S. Liu, Y. B. Yang, J. H. Zhang, and Y. Zhao, arXiv:1803.04393.
[42] W. Wang, S. Zhao, and R. Zhu, Eur. Phys. J. C **78**, 147 (2018).
[43] W. Wang and S. Zhao, J. High Energy Phys. 05 (2018) 142.
[44] H. W. Lin, J. W. Chen, X. Ji, L. Jin, R. Li, Y. S. Liu, Y. B. Yang, J. H. Zhang, and Y. Zhao, Phys. Rev. Lett. **121**, 242003 (2018).
[45] Y. S. Liu *et al.* (Lattice Parton Collaboration), Phys. Rev. D **101**, 034020 (2020).
[46] C. Alexandrou, K. Cichy, M. Constantinou, K. Jansen, A. Scapellato, and F. Steffens, Phys. Rev. D **98**, 091503 (2018).
[47] Y. S. Liu, J. W. Chen, L. Jin, R. Li, H. W. Lin, Y. B. Yang, J. H. Zhang, and Y. Zhao, arXiv:1810.05043.
[48] J. H. Zhang, J. W. Chen, L. Jin, H. W. Lin, A. Schäfer, and Y. Zhao, Phys. Rev. D **100**, 034505 (2019).
[49] T. Izubuchi, L. Jin, C. Kallidonis, N. Karthik, S. Mukherjee, P. Petreczky, C. Shugert, and S. Syritsyn, Phys. Rev. D **100**, 034516 (2019).
[50] L. B. Chen, W. Wang, and R. Zhu, Phys. Rev. D **102**, 011503 (2020).
[51] L. B. Chen, W. Wang, and R. Zhu, J. High Energy Phys. 10 (2020) 079.
[52] L. B. Chen, W. Wang, and R. Zhu, Phys. Rev. Lett. **126**, 072002 (2021).
[53] C. Shugert, X. Gao, T. Izubichi, L. Jin, C. Kallidonis, N. Karthik, S. Mukherjee, P. Petreczky, S. Syritsyn, and Y. Zhao, arXiv:2001.11650.
[54] Y. Chai, Y. Li, S. Xia, C. Alexandrou, K. Cichy, M. Constantinou, X. Feng, K. Hadjiyiannakou, K. Jansen, and G. Koutsou *et al.*, Phys. Rev. D **102**, 014508 (2020).
[55] H. W. Lin, J. W. Chen, Z. Fan, J. H. Zhang, and R. Zhang, Phys. Rev. D **103**, 014516 (2021).
[56] Z. Fan, X. Gao, R. Li, H. W. Lin, N. Karthik, S. Mukherjee, P. Petreczky, S. Syritsyn, Y. B. Yang, and R. Zhang, Phys. Rev. D **102**, 074504 (2020).
[57] X. Gao, K. Lee, S. Mukherjee, C. Shugert, and Y. Zhao, Phys. Rev. D **103**, 094504 (2021).
[58] X. Gao, A. D. Hanlon, S. Mukherjee, P. Petreczky, P. Scior, S. Syritsyn, and Y. Zhao, Phys. Rev. Lett. **128**, 142003 (2022).
[59] X. Gao, A. D. Hanlon, N. Karthik, S. Mukherjee, P. Petreczky, P. Scior, S. Shi, S. Syritsyn, Y. Zhao, and K. Zhou, Phys. Rev. D **106**, 114510 (2022).
[60] Y. Su, J. Holligan, X. Ji, F. Yao, J. H. Zhang, and R. Zhang, Nucl. Phys. **B991**, 116201 (2023).
[61] F. Yao *et al.* (Lattice Parton Collaboration), Phys. Rev. Lett. **131**, 261901 (2023).
[62] X. Gao, A. D. Hanlon, J. Holligan, N. Karthik, S. Mukherjee, P. Petreczky, S. Syritsyn, and Y. Zhao, Phys. Rev. D **107**, 074509 (2023).
[63] X. Gao, A. D. Hanlon, S. Mukherjee, P. Petreczky, Q. Shi, S. Syritsyn, and Y. Zhao, Phys. Rev. D **109**, 054506 (2024).
[64] X. Gao, W. Y. Liu, and Y. Zhao, Phys. Rev. D **109**, 094506 (2024).
[65] C. Chen, Y. Geng, L. Liu, P. Sun, Y.-B. Yang, F. Yao, J.-H. Zhang, and K. Zhang (CLQCD and Lattice Parton Collaborations), Phys. Rev. D **111**, 074506 (2025).
[66] J. Holligan and H. W. Lin, J. Phys. G **51**, 065101 (2024).
[67] J. Holligan and H. W. Lin, Phys. Lett. B **854**, 138731 (2024).
[68] M. Constantinou and H. Panagopoulos, Phys. Rev. D **96**, 054506 (2017).
[69] I. W. Stewart and Y. Zhao, Phys. Rev. D **97**, 054512 (2018).
[70] K. Zhang, Y.-K. Huo, X. Ji, A. Schäfer, C.-J. Shi, P. Sun, W. Wang, Y.-B. Yang, and J.-H. Zhang (Lattice Parton Collaboration), Phys. Rev. D **110**, 074505 (2024).
[71] Y. K. Huo *et al.* (Lattice Parton (LPC) Collaboration), Nucl. Phys. **B969**, 115443 (2021).
[72] X. Ji, Y. Liu, A. Schäfer, W. Wang, Y. B. Yang, J. H. Zhang, and Y. Zhao, Nucl. Phys. **B964**, 115311 (2021).
[73] C. Y. Chou and J. W. Chen, Phys. Rev. D **106**, 014507 (2022).
[74] R. Narayanan and H. Neuberger, J. High Energy Phys. 03 (2006) 064.
[75] M. Lüscher, J. High Energy Phys. 08 (2010) 071; 03 (2014) 92.
[76] M. Luscher and P. Weisz, J. High Energy Phys. 02 (2011) 051.
[77] M. Luscher, J. High Energy Phys. 04 (2013) 123.
[78] C. Monahan and K. Orginos, EPJ Web Conf. **175**, 06004 (2018).
[79] C. Monahan, Phys. Rev. D **97**, 054507 (2018).
[80] N. Brambilla and X. P. Wang, J. High Energy Phys. 06 (2024) 210.
[81] A. NieMiera, W. Good, H. W. Lin, and F. Yao, arXiv: 2510.17758.

[82] A. Francis, P. Fritzsch, R. Karur, J. Kim, G. Pederiva, D. A. Pefkou, A. Rago, A. Shindler, A. Walker-Loud, and S. Zafeiropoulos, arXiv:2510.26738.
[83] A. Francis, P. Fritzsch, R. V. Harlander, R. Karur, J. Kim, J. T. Kohnen, G. Pederiva, D. A. Pefkou, A. Rago, and A. Shindler *et al.*, arXiv:2509.02472.
[84] V. M. Braun, S. E. Derkachov, G. P. Korchemsky, and A. N. Manashov, Nucl. Phys. **B553**, 355 (1999).
[85] V. Braun, R. J. Fries, N. Mahnke, and E. Stein, Nucl. Phys. **B589**, 381 (2000); **B607**, 433(E) (2001).
[86] M. Luscher, Commun. Math. Phys. **293**, 899 (2010).
[87] M. Lüscher, Proc. Sci. LATTICE2013 (**2014**) 016 [arXiv:1308.5598].
[88] S. Borsányi *et al.* (BMW Collaboration), J. High Energy Phys. 09 (2012) 010.
[89] R. Sommer, Proc. Sci. LATTICE2013 (**2014**) 015 [arXiv:1401.3270].
[90] H. Suzuki, Prog. Theor. Exp. Phys. **2013**, 083B03 (2013); **2015**, 079201(E) (2015).
[91] H. Makino and H. Suzuki, Prog. Theor. Exp. Phys. **2014**, 63B02 (2014); **2015**, 079202(E) (2015).
[92] R. V. Harlander, Y. Kluth, and F. Lange, Eur. Phys. J. C **78**, 944 (2018); **79**, 858(E) (2019).
[93] Y. Aoki *et al.* (Flavour Lattice Averaging Group (FLAG)), arXiv:2411.04268.
[94] V. Leino, N. Brambilla, J. Mayer-Steudte, and A. Vairo, EPJ Web Conf. **258**, 04009 (2022).
[95] J. Mayer-Steudte, N. Brambilla, V. Leino, and A. Vairo, Proc. Sci. LATTICE2022 (**2023**) 353 [arXiv:2212.12400].
[96] V. Leino, N. Brambilla, J. Mayer-Steudte, and P. Petreczky, Proc. Sci. LATTICE2022 (**2023**) 183 [arXiv:2212.10941].
[97] M. Nagatsuka, K. Sakai, and S. Sasaki, Phys. Rev. D **108**, 094506 (2023).
[98] F. Lange, Dissertation, RWTH Aachen University, 2021, 10.18154/RWTH-2021-07652.
[99] C. Monahan and K. Orginos, J. High Energy Phys. 03 (2017) 116.
[100] M. Beneke, Phys. Rep. **317**, 1 (1999).
[101] M. Beneke and V. M. Braun, Nucl. Phys. **B426**, 301 (1994).
[102] J. L. Zhang, Phys. Rev. D **112**, 094504 (2025).
[103] K. Orginos, A. Radyushkin, J. Karpie, and S. Zafeiropoulos, Phys. Rev. D **96**, 094503 (2017).
[104] A. V. Radyushkin, Phys. Lett. B **781**, 433 (2018).
[105] H. Bai *et al.* (LPC Collaboration), arXiv:2508.08971.